

# Numerical predictions of two-dimensional conduction, convection, and radiation heat transfer. I. Formulation

Daniel R. Rousse \*

Département de génie mécanique-Université Laval, Cité Universitaire, Québec, Canada G1K 7P4

(Received 4 March 1999, accepted 26 August 1999)

**Abstract** — The research presented in this paper involves the detailed formulation of a Control-Volume Finite Element Method (CVFEM) for the solution of combined-mode heat transfer in participating media. The proposed numerical method accounts for emitting, absorbing, and scattering media in regularly- and irregularly-shaped geometries. In the proposed CVFEM, the calculation domain is divided into three-node triangular finite elements: the geometrical flexibility associated with finite element methods is preserved. Each element is further subdivided in such a way that upon assembly of all elements, complete control volumes are formed around each node in the calculation domain. To account for the directional nature of radiation heat transfer, a spherical envelope, surrounding each node in the calculation domain, is discretized in adjacent non-overlapping solid angles (or control angles). Element-based interpolation functions for the dependent variables, and the subdomain-type method of weighted residuals are used to derive algebraic approximations to the governing equations. Interpolation schemes that guarantee positive contributions to the coefficients in the algebraic discretization equations are used to approximate the convective and radiative fluxes across control-volume surfaces. © 2000 Éditions scientifiques et médicales Elsevier SAS

control volume finite elements method / discrete ordinates / combined modes heat transfer / two-dimensional / formulation

**Résumé** — Prédiction numérique du transfert par conduction, convection et rayonnement thermiques. I. Formulation. La recherche présentée dans cet article implique la formulation détaillée d'une Méthode d'Éléments Finis basée sur des Volumes de Contrôle (MEFVC) pour la résolution du transfert thermique combiné dans des milieux semi-transparents. La méthode numérique proposée permet de tenir compte de milieux qui émettent, absorbent et diffusent le rayonnement dans des géométries irrégulières ou non. Dans la MEFVC proposée, le domaine de calcul est d'abord divisé en éléments triangulaires : la flexibilité géométrique associée aux éléments finis est préservée. Chaque élément est subdivisé de façon à former des volumes de contrôle polygonaux autour de chaque noeud du domaine de calcul. Pour tenir compte de la directionnalité de l'intensité du rayonnement, une enveloppe sphérique autour de chaque noeud est discrétisée en angles solides adjacents. Des fonctions d'interpolation élémentaires et une méthode des résidus pondérés en sous-domaines sont utilisées pour dériver les équations de discrétisation. Des schémas d'interpolation qui garantissent des contributions positives aux coefficients des équations de discrétisation algébriques sont employés. © 2000 Éditions scientifiques et médicales Elsevier SAS

méthode éléments finis volumes de contrôle / ordonnées discrètes / modes combinés de transfert thermique / bi-dimensionnel / formulation

## Nomenclature

$A$	coefficient of the discretization equation, surface area		$N$	Stark number, number of panels defining a control volume	
$c_p$	medium specific heat . . . . .	$J \cdot kg^{-1} \cdot K^{-1}$	$\vec{n}$	unit vector normal to a surface	
$e$	emissive power . . . . .	$W \cdot m^{-2}$	$p$	control volume surface (panel)	
$g$	incident radiant energy . . . . .	$W \cdot m^{-2}$	$Pe$	Peclet number	
$i$	radiative intensity . . . . .	$W \cdot m^{-2} \cdot sr^{-1}$	$\vec{q}$	heat flux . . . . .	$W \cdot m^{-2}$
$\vec{J}$	dimensionless flux (conductive, convective or radiative)		$q'''$	internal heat generation . . . . .	$W \cdot m^{-3}$
$k$	medium conductivity . . . . .	$W \cdot m^{-1} \cdot K^{-1}$	$Q_I^m$	impinging dimensionless radiative flux	
			$Q_B^{in}$	total incoming dimensionless radiative flux	
			$r$	reference point for RTE integration	
			$s$	spatial position . . . . .	m
			$S_\phi$	rate of volumetric generation of $\phi$	
			$S_I$	source of radiative intensity	

\*Daniel.Rousse@gmc.ulaval.ca

$T$	temperature . . . . .	K
$\vec{u}$	velocity . . . . .	$\text{m}\cdot\text{s}^{-1}$
$V$	volume . . . . .	$\text{m}^3$
$x$	independent variable	
$y$	independent variable	

*Greek symbols*

$\beta$	extinction coefficient . . . . .	$\text{m}^{-1}$
$\epsilon$	emissivity of a surface	
$\gamma$	albedo for single scattering	
$\kappa$	absorption coefficient . . . . .	$\text{m}^{-1}$
$\hat{\omega}$	solid angle . . . . .	sr
$\vec{\Omega}$	direction of propagation	
$\phi$	dependent variable	
$\Phi$	phase function for scattering	
$\mu, \eta, \xi$	direction cosines of $\vec{\Omega}$	
$\xi$	independent variable	
$\rho$	medium density . . . . .	$\text{kg}\cdot\text{m}^{-3}$
$\sigma$	scattering coefficient . . . . .	$\text{m}^{-1}$
$\tilde{\sigma}$	Stefan–Boltzmann constant, 5.67051E–8 . . . . .	$\text{W}\cdot\text{m}^{-2}\cdot\text{K}^{-4}$
$\tau$	optical depth	
$\tau_0$	optical thickness	

*Subscripts*

*	reference quantity
b	black body
B	boundary
C	constant (part of the source term)
$l$	control volume surface (panel)
$m$	discrete direction
$P$	node of reference
$r$	radiation, or reference point
e	element
$\vartheta$	integer used in the node location

*Superscripts*

*	evaluated at a preceeding step of an iterative procedure
$\vec{\phantom{x}}$	vectorial quantity
$\prime$	incoming direction
$\bar{\phantom{x}}$	bulk value
$\tilde{\phantom{x}}$	modified quantity
$\hat{\phantom{x}}$	geometric quantity
C	convection term
D	diffusion term

## 1. INTRODUCTION

Efficient designs of furnaces, ovens and combustion chambers call for numerical methods capable of solving

problems that involve conduction, convection, and radiation, or combined modes of heat transfer.

### 1.1. Classical methods

In this context, several general methods have been put forward to investigate multidimensional radiative transport in participating media. Among them, the zonal method [1, 2] and the Monte-Carlo method [3–5] have long been accepted as the most accurate methods for the calculation of radiative heat transfer. However, it is now well established that both these methods have been proved difficult to incorporate in other discrete numerical methods for conduction and convection heat transfer, and that they require a large amount of computational time and storage capacity. Consequently, alternate ways have been considered for the calculation of radiative heat transfer in the context of practical applications.

### 1.2. $P_N$ methods

$P_N$  methods received much attention and were implemented in commercial codes such as FIDAP [6] but the formulation of higher order approximations than  $P_1$ —which is not a very accurate method—is complicated and their implementation leads to important computational times without substantial gain in accuracy [7].

To be embedded in a comprehensive numerical method, a suitable discretization method for radiation should: (1) permit compatibility with available methods that solve fluid flow and convective heat transfer; (2) allow geometrical flexibility; (3) account for absorption, emission, and anisotropic scattering; and (4) be affordable. In this respect, there exist two competing methods that share many researchers interest: the Discrete Transfer Method (DTM) and the Discrete Ordinates Methods (DOM), and their variations and improvements.

### 1.3. Discrete transfer method

The DTM [8] offers several interesting features as it incorporates key ideas of the Zonal, Monte-Carlo, and flux methods. It also readily satisfies three of the four above-mentioned characteristics. In a paper by Meng et al. [9], the authors successfully implemented the method on an unstructured mesh, but confirmed the conclusion reported by Carvalho et al. [10] that the method does not yet provide high accuracy for scattering media. In a study

by Selçuk and Kayakol [11] the investigators evaluated the method in applications dealing with combustors and reported similar conclusions.

#### 1.4. Discrete ordinates method

The DOM [12–15] also satisfies three of the four above-mentioned characteristics. Ramankutty and Crosbie [16] present an exhaustive survey of successful investigations relating to the DOM in two-dimensional rectangular enclosures that include scattering. Selçuk and Kayakol [17] evaluated the method in applications dealing with rectangular furnaces and recommended to use it in lieu of the DTM. The method was implemented in the Finite Difference Method (FDM) [13]; in the Finite Volume Method (FVM) [15, 18–22]; and recently in the Finite Element Method [23]. The method was implemented in both two- and three-dimensional Cartesian enclosures and also successfully in cylindrical enclosures by Jamaluddin and Smith [24, 25]. Today, the method is used in various applications such as the computation of radiant heat loss from diesel engines [26] or radiative transfer in composite materials with Fresnel boundaries [27].

#### 1.5. Irregular geometries

The DOM was mostly implemented in geometries into which the solid angle edges coincided with the physical boundaries of the domain, namely into Cartesian or cylindrical geometries. There is however a problem when it comes to solve for irregularly-shaped physical domains.

To handle irregular geometries, Liu et al. [28] proposed to solve the RTE with the DOM in general body-fitted coordinates (BFC). They also recommended the use of a general FVM instead of a FVM based DOM and they showed the differences between the two types of methods. Following the work of Fiveland and Jessee [23], an even-parity (EP) formulation of the DOM in BFC has also been proposed by Liu et al. [29] but it was found less interesting than the standard formulation. Nevertheless, the same authors [30] proposed to solve the EP-DOM in BFC. In this paper, the authors compare a standard RTE formulation with the EP-RTE formulation and also conclude that the conventional DOM formulation should be used. In another interesting effort to handle irregular geometries, Vaillon et al. [31] adapted the DOM to solve the RTE in orthogonal curvilinear coordinates. Charette

et al. [32] proposed a new DOM that uses general characteristic relations instead of standard differencing schemes which involve a skew exponential scheme at the elemental level.

To account for irregular geometries, Chui [33] and co-workers [34–37] proposed FVMs which involve the discretization of the sphere surrounding each node of the computational domain according to an azimuthal  $\phi$ - $\theta$  pattern. This discretization into control-angles is particularly suitable for some irregularly-shaped two-dimensional domains. There is an interesting feature in the proposed formulation: it does not depend on quadratures to evaluate the angular integrals. The value of  $\int (\hat{\Omega} \cdot \hat{\nabla}) d\hat{\omega}$  can be computed. Thus, the angular discretization is not necessarily rigid and restricted as in DOM. Chai and co-workers formulated both general FVMs and FVM based DOMs: in [38] an improved treatment of scattering was proposed for the DOM, in [39] spatial interpolation schemes were evaluated, in [40] a FVM was proposed partly based on Raithby and Chui's work [34, 37], in [41, 42] the issue of irregularly-shaped domains was considered. Recently, Chai and Moder [43] proposed yet another interesting avenue for the treatment of irregular domains: a spatial multiblock procedure in a FVM formulation. Blocked-off region procedures have been proposed by Sanchez and Smith [44] and by Adams and Smith [45] for the same purpose.

#### 1.6. Control volume finite element methods

Since the first publication by Baliga and Patankar [46], the CVFEM has been the focus of a variety of studies. For example, Ferguson and Turner [47] used a CVFEM to analyse the drying-induced stresses in timber. There is also a good deal of recent work involving improvement of the method: Larreteguy [48] used the original formulation and also proposed an enhancement of the interpolation function of the convection term; Padra and Larreteguy [49] proposed an a-posteriori error estimator for the CVFEM as applied to convection–diffusion problems; Harms et al. [50] suggested a simplified formulation of a two-dimensional CVFEM based on quadrilateral elements; and Comini et al. [51] concluded that CVFEM performs better than Bubnov–Galerkin methods with four-node bilinear elements. A detailed discussion of similarities and differences among control volume based methods (including FVMs and CVFEMs) was proposed in the review paper by Prakash and Baliga [52].

The work of Rousse et al. [53–60] was intended to bridge the gap between successful CVFEM for fluid flow and heat transfer and the need for a method that numerically solves the RTE. In [53], the formulation of a CVFEM for the solution of two-dimensional problems in rectangular geometries was proposed; in [54] the validation of the above-mentioned CVFEM was carried out; in [55] the method was extended to combined-mode problems; and in [56, 60] the method was applied to situations involving multidimensional combined-mode problems. The capabilities and limitations of the CVFEM formulation were discussed in [57].

## 1.7. Objectives

The aim of this paper is to present in *detail* a multidimensional CVFEM for the solution of the equations that govern combined modes of heat transfer, including radiative heat transfer, in a fluid medium that emits, absorbs and scatters thermal radiation, within irregularly-shaped geometries. Guidance for the formulation of a solution procedure for radiation heat transfer has been obtained from the discrete ordinates formulation originally proposed by Chandrasekhar [12], and those employed by Carlson and Lathrop [13], Fiveland [15], and Hyde and Truelove [14, 61]. This CVFEM, based on the original efforts of Baliga [62], and Baliga and Patankar [46, 63], also shares some of the ideas involved with the FVM formulation of Chui and Raithby [33, 34, 37]. Some of the capabilities of this CVFEM are demonstrated in a companion paper [64] by its application to different test problems. The research presented in this paper is related to the first research effort to incorporate a facility for the calculation of radiation heat transfer in participating media into a CVFEM for fluid flow problems.

## 1.8. Contents of the paper

In the remainder of this paper the complete formulation of the proposed two-dimensional CVFEM is presented, with emphasis on the radiation aspect. The mathematical model is presented first, then spatial and angular discretization details are enunciated followed by sections that discuss the conservation equations, the interpolation functions, and the discretization equations. The boundary-condition contributions, and the solution procedure of the proposed CVFEM are given in the last sections of the paper.

## 2. GOVERNING EQUATIONS

Consider steady conduction, convection, and radiation in a single-phase, incompressible, Newtonian fluid within a gray-diffuse opaque enclosure. The fluid participates in the radiation process, and it is assumed to be gray, isotropic, and in local thermodynamic equilibrium (LTE). In addition, its thermophysical and radiative properties are assumed to remain constant. Fourier's law of heat conduction applies, and viscous dissipation is neglected. With respect to these assumptions, the steady-state energy equation simplifies to

$$\rho c_p \vec{\nabla} \cdot (\vec{u}(s)T(s)) = k \nabla^2 T(s) - \vec{\nabla} \cdot \vec{q}_r(s) + q'''(s) \quad (1)$$

where the first term accounts for the rate of advection, the second term represents the rate of heat conduction, the third term is related to the rate of radiation heat transfer, and the last term describes the rate of internal heat generation per unit volume within the medium.

The multidimensional propagation of thermal radiation in gray-diffuse opaque enclosures, filled with constant properties gray participating media in local thermodynamic equilibrium and unit refractive index, can be described by the following equation:

$$\begin{aligned} \vec{\nabla} \cdot (\vec{\Omega} i(s, \vec{\Omega})) &= -\beta(s) i(s, \vec{\Omega}) + \kappa(s) i_b(s, \vec{\Omega}) \\ &+ \frac{\sigma(s)}{4\pi} \int_{4\pi} i(s, \vec{\Omega}') \Phi(\vec{\Omega}' \Rightarrow \vec{\Omega}) d\omega' \end{aligned} \quad (2)$$

where the first term,  $\vec{\nabla} \cdot (\vec{\Omega} i(s, \vec{\Omega}))$ , accounts for the variation of the radiant intensity  $i(s, \vec{\Omega})$  at a point  $s$  along a direction  $\vec{\Omega}$ ; the term  $-\beta i(s, \vec{\Omega})$  represents the attenuation (extinction) in the same direction by absorption and scattering at position  $s$  in the medium; the following term involves local emission of radiation at  $s$  along direction  $\vec{\Omega}$ ; and the last term describes the scattering in direction  $\vec{\Omega}$  of incident radiation from all other directions, denoted by  $\vec{\Omega}'$ , at point  $s$ .

The radiative boundary condition at a point  $B$  on a gray-diffuse surface is given by the following equation:

$$\begin{aligned} i(B, \vec{\Omega}) &= \epsilon(B) i_b(B, \vec{\Omega}) + \frac{[1 - \epsilon(B)]}{\pi} \\ &\cdot \int_{[\vec{\Omega}' \cdot \vec{n}(B)] < 0} |\vec{\Omega}' \cdot \vec{n}(B)| i(B, \vec{\Omega}') d\omega' \end{aligned} \quad (3)$$

where  $i(B, \vec{\Omega})$  is the total intensity (emitted plus reflected) directed inside the investigated domain; the term  $\epsilon(B) i_b(B, \vec{\Omega})$  accounts for emission of intensity at  $B$  into the domain; and the last term represents the reflected

part of the incident radiation impinging on the boundary point  $B$ , from all directions.

The divergence of the radiative flux vector in equation (1),  $\vec{\nabla} \cdot \vec{q}_r(s)$ , characterizes the net efflux of radiant energy from a unit volume per unit time over all wavelengths. In a *gray* participating medium, the divergence of the radiative flux vector  $\vec{\nabla} \cdot \vec{q}_r(s)$  at a location  $s$ , is a linear function of the excess of the local black-body emissive power,  $e_b(s)$ , over the local incident radiant energy,  $g(s)$ . It is evaluated by the following equation:

$$\vec{\nabla} \cdot \vec{q}_r(s) = \kappa(s)[4e_b(s) - g(s)] \quad (4)$$

where  $\kappa(s)$  is the absorption coefficient of the medium at  $s$ , and  $e_b(s) = \tilde{\sigma} T^4(s)$  and  $g(s) = \int_{4\pi} i(s, \vec{\Omega}) d\hat{\omega}$ .

## 2.1. Dimensionless mathematical model

The independent space variable  $s$  can be nondimensionalized with respect to: (1) the extinction coefficient,  $\beta$ , or (2) an optical depth,  $\tau$ , and a characteristic length,  $L_*$  ( $\tau = \beta L_*$ ). The angular variable  $\hat{\omega}$  associated with direction  $\vec{\Omega}$  can conveniently be divided by the solid angle subtended by the surface of a unit sphere at its center,  $4\pi$ . This yields:

$$S = \beta s = \tau \frac{s}{L_*} \quad \text{and} \quad \omega = \frac{\hat{\omega}}{4\pi} \quad (5)$$

Employing a reference velocity,  $u_*$ , a reference absolute temperature,  $T_*$ , and the following dimensionless variables

$$\begin{aligned} \vec{U} &= \frac{\vec{u}}{u_*}; & \Theta &= \frac{T}{T_*}; & Q''' &= \frac{q'''}{4\tilde{\sigma} T_*^4 \beta} \\ I &= \frac{i\pi}{\tilde{\sigma} T_*^4}; & \vec{Q}_r &= \frac{\vec{q}_r}{4\tilde{\sigma} T_*^4}; & E_b &= \frac{e_b}{\tilde{\sigma} T_*^4} \\ G &= \frac{g}{4\tilde{\sigma} T_*^4} \end{aligned} \quad (6)$$

the set of coupled governing equations for combined-modes problems can be expressed as follows:

$$\frac{Pe}{\tau} \vec{\nabla} \cdot (\vec{U}(S)\Theta(S)) = \nabla^2 \Theta(S) - \frac{1}{N} \vec{\nabla} \cdot \vec{Q}_r(S) + \frac{1}{N} Q'''(S) \quad (7)$$

$$\vec{\nabla} \cdot (\vec{\Omega} I(S, \vec{\Omega})) = -I(S, \vec{\Omega}) + S_I(S, \vec{\Omega}) d\omega' \quad (8)$$

with a source function for radiant intensity  $S_I(S, \vec{\Omega})$  defined as [66]

$$\begin{aligned} S_I(S, \vec{\Omega}) &= (1 - \gamma(S)) I_b(S, \vec{\Omega}) \\ &+ \gamma(S) \int_1 I(S, \vec{\Omega}') \Phi(\vec{\Omega} \Rightarrow \vec{\Omega}) d\omega' \end{aligned} \quad (9)$$

The influence of radiation heat transfer within the energy equation is accounted for via:

$$\vec{\nabla} \cdot \vec{Q}_r(S) = (1 - \gamma(S)) [E_b(S) - G(S)] \quad (10)$$

where  $E_b(S) = \Theta^4(S)$  and  $G(S) = \int_1 I(S, \vec{\Omega}) d\omega$ .

Finally, the dimensionless radiative boundary condition at a point  $B$  on a gray-diffuse surface is given by the following equation [65]:

$$\begin{aligned} I(B, \vec{\Omega}) &= \epsilon(B) I_b(B, \vec{\Omega}) + 4(1 - \epsilon(B)) \\ &\cdot \int_{[\vec{\Omega}' \cdot \vec{n}(B)] < 0} |\vec{\Omega}' \cdot \vec{n}(B)| I(B, \vec{\Omega}') d\omega' \end{aligned} \quad (11)$$

In equations (7)–(10), the Stark number,  $N$ ; the Peclet number,  $Pe$ ; and the albedo for single scattering,  $\gamma$ , are dimensionless parameters defined by the following expressions:

$$\begin{aligned} N &= \frac{k\beta}{4\tilde{\sigma} T_*^3}; & Pe &= \frac{\rho c_p u_* L_*}{k} \\ \gamma(S) &= \frac{\sigma(S)}{\beta(S)} \end{aligned} \quad (12)$$

## 2.2. The general differential equation

In the formulation of the present CVFEM, it is convenient to cast the governing differential equations in the following general form [67]:

$$\vec{\nabla} \cdot \vec{J}_\phi = S_\phi \quad (13)$$

where  $\phi$  stands for a general dependent variable,  $S_\phi$  is a volumetric generation rate or *source* term, and  $\vec{J}_\phi$  is the flux of  $\phi$ . Equations (7) and (8) may be obtained from this general equation by using the expressions given in *table I* for radiative heat transfer and combined conduction, convection and radiation heat transfer, respectively. This table also provides the expressions of  $\vec{J}_\phi$  and  $S_\phi$  in the context of pure convection–diffusion problems and conduction–radiation problems.

TABLE I  
Expressions of  $\vec{J}_\phi$  and  $S_\phi$  for several typical problems.

Problem	$\vec{J}_\phi$	$S_\phi$
Conduction + Convection	$Pe\vec{U}(S)\Theta(S) - \vec{\nabla}\Theta(S)$	$Q'''(S)$
Radiation	$\vec{\Omega}I(S, \vec{\Omega})$	$-I(S, \vec{\Omega}) + S_I(S, \vec{\Omega})$
Conduction + Radiation	$\vec{\nabla}\Theta(S)$	$-(1/N)(Q'''(S) - \vec{\nabla} \cdot \vec{Q}_r(S))$
Cond. + Conv. + Rad.	$(Pe/\tau)\vec{U}(S)\Theta(S) - \vec{\nabla}\Theta(S)$	$(1/N)(Q'''(S) - \vec{\nabla} \cdot \vec{Q}_r(S))$

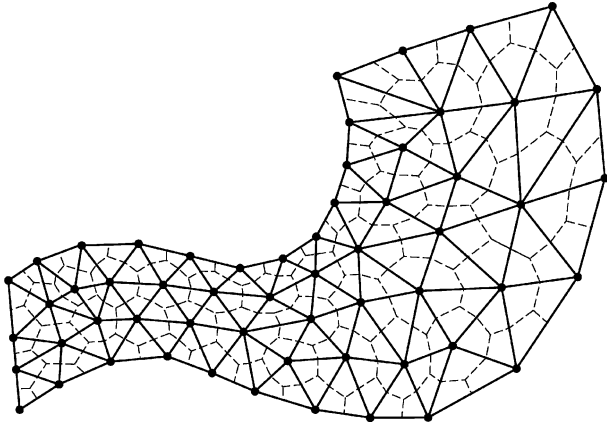


Figure 1. Spatial discretization of two-dimensional planar domains.

### 3. SPATIAL DISCRETIZATION OF THE DOMAIN

In CVFEMs, the calculation domain is first spatially divided into elements. Then, within each element, sub-control volumes of equal size are defined in such a manner that upon assembly of all elements, control volumes are formed around each node in the calculation domain. These control volumes do not overlap, and collectively, they fill the physical domain exactly and completely. All dependent variables in the CVFEM presented in this work are stored at the same grid points of the finite element mesh (co-located).

In the proposed two-dimensional planar CVFEM, three-node triangular elements are first employed to divide the domain. Then, in a further discretization, the centroids of the elements are joined to the midpoints of the corresponding sides; this creates polygonal control volumes surrounding each grid point of the mesh. A sample irregularly-shaped two-dimensional domain discretization is shown in *figure 1*: here, the solid lines denote the domain and element boundaries and the dashed lines the control volume faces.

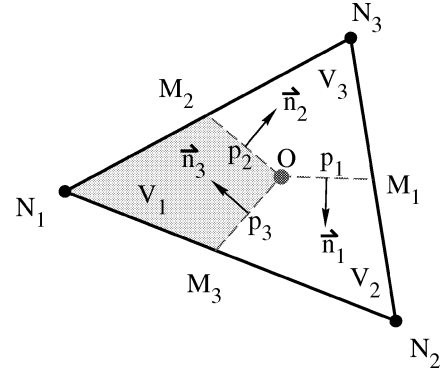


Figure 2. Element subdivision into equal-weight sub-control volumes and notation.

### 3.1. Implementation

The calculation domains in the problems presented in the companion paper by Rousse et al. [64] were discretized using a line-by-line structured grid scheme, which facilitates the storage and assembly of the coefficients in the discretization equations. However, implementation on structured grids is by no means an intrinsic limitation of the CVFEM involved in this work.

Referring to the element schematically depicted in *figure 2*, the centroid  $O$  is joined to the midpoints, denoted by  $M_1$ ,  $M_2$ , and  $M_3$ , of the element edges. This gives birth to equal-size [62] sub-control volumes,  $V_1$ ,  $V_2$ , and  $V_3$ . The nodes are denoted by  $N_1$ ,  $N_2$ , and  $N_3$  for each element, in the counter-clockwise direction with respect to the centroid. Panels,  $p_1$ ,  $p_2$ , and  $p_3$ , have their associated unit normals,  $\vec{n}_1$ ,  $\vec{n}_2$ , and  $\vec{n}_3$ , defined to point in the clockwise direction with respect to  $O$ .

### 4. ANGULAR DISCRETIZATION OF THE DOMAIN

In this work, it is necessary to consider the directional discretization of a spherical envelope around *each* grid point of the spatially discretized domain. Each of these

spherical envelopes is subdivided into  $M$  discrete contiguous solid angles,  $\omega_m$ , each associated with a corresponding discrete direction,  $\vec{\Omega}_m$ . These solid angles (or control angles) do not overlap and collectively they span the sphere exactly and completely. To ensure consistency, the angular discretization for each grid node is the same in size, distribution, and orientation.

#### 4.1. Implementation

There is no optimum type of discretization for all situations. Completely symmetric angular discretizations [13, 18, 61] are frequently preferred in regularly-shaped geometries because of their accuracy; special angular discretizations are used only to satisfy particular conditions that increase accuracy or meet geometric requirements. In the proposed method, two different discretizations are formulated and implemented: (1) equal-weight (EW) solid angles,  $\omega_m$ , are employed in regular geometries. This discretization, used in combination with  $S_N$ -type discretization, leads to the  $EW S_N$  discretization; (2) azimuthal discretization according to the azimuthal angle  $\phi$

measured in the plane of interest and the polar angle  $\theta$  measured with respect to the normal to the plane of interest. *Figure 3* schematically shows the two types of angular discretizations used.

For angular discretization, the CVFEM does not impose restrictions on the size and the numbers of solid angles,  $\omega_m$ , and the orientation of the discrete directions  $\vec{\Omega}_m$ . However, care must be taken to ensure consistency (zeroth and first full-range moments when discretizing using  $S_n$  angular discretization) and energy conservation at the boundaries (half-range first moment as discussed by Fiveland [18] and Truelove [61]).

#### 5. CONSERVATION EQUATIONS

Applied to an arbitrary control volume  $V$ , fixed in space, and to a given solid angle  $\omega_m$ , the integral formulation of the steady general differential equation, equation (13) is

$$\int_{\omega_m} \int_A \vec{J}_\phi \cdot \vec{n} \, dA \, d\omega = \int_{\omega_m} \int_V S_\phi \, dV \, d\omega \quad (14)$$

where  $A$  is the surface area of the control volume, and  $\vec{n}$  is a unit *outward-pointing* normal to the differential area element  $dA$ . One should note that for the energy equation, equation (7),  $\vec{J}_\phi$  and  $S_\phi$  are independent of direction  $\vec{\Omega}$ , and that the integral over solid angles is unnecessary. In the formulation, the convection–diffusion flux of  $\phi$  is expressed as

$$\vec{J}_\phi = \vec{J}_\phi^C + \vec{J}_\phi^D = \frac{Pe}{\tau} \vec{U} \phi - \vec{\nabla} \phi \quad (15)$$

because the interpolation functions used for  $\vec{J}_\phi^C$  and  $\vec{J}_\phi^D$  differ.

In two-dimensional planar geometries, consider the integral conservation equation as applied to the polygonal control volume surrounding node  $N_1$  and to a solid angle  $\omega_m$  in *figure 2*. With respect to the notation involved in this figure, equation (14) can be represented by the following statement:

$$\begin{aligned} & \left[ \int_{\omega_m} \int_{p_2} (\vec{J}_\phi \cdot \vec{n}_2) \, dA \, d\omega - \int_{\omega_m} \int_{p_3} (\vec{J}_\phi \cdot \vec{n}_3) \, dA \, d\omega \right. \\ & \quad \left. - \int_{\omega_m} \int_{V_1} S_\phi \, dV \, d\omega \right] \\ & + [\text{similar contributions from other elements linked with } N_1] \\ & + [\text{boundary contributions, if applicable}] = 0 \quad (16) \end{aligned}$$

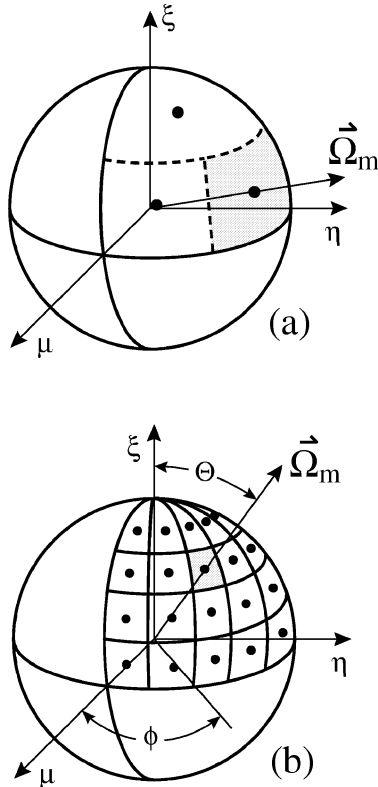


**Figure 3.** Angular discretization. (a)  $S_n$ -type discretization; (b) azimuthal  $\phi$ - $\theta$ -type discretization.

in which the first square-bracketed expression on the left-hand side describes the contribution of sub-control volume,  $V_1$ , to the full control volume conservation equation for node  $N_1$ .

## 6. INTERPOLATION FUNCTIONS

### 6.1. Thermophysical and radiative properties

In the suggested CVFEM, the albedo for scattering,  $\gamma(S)$ , and the scattering phase function,  $\Phi(\vec{\Omega}' \Rightarrow \vec{\Omega})$ , are evaluated at the grid point of the finite element mesh and are assumed to prevail over the control volume associated with this point.  $\gamma(S)$  is an isotropic property while  $\Phi(\vec{\Omega}' \Rightarrow \vec{\Omega})$  can change with direction. Both the albedo and the phase function are also assumed to prevail over a solid angle  $\omega$ . All other thermophysical properties,  $k$ ,  $c_p$ ,  $\rho$ , are evaluated at the centroid of an element and are assumed to prevail over that element.

### 6.2. Volumetric source terms

In the interpolation of the volumetric source term  $S_\phi$  of equation (7), it is appropriate to linearize the components of the term that involves  $\vec{\nabla} \cdot \vec{Q}_r$ . In this situation, the coefficients of the linearized source term are computed at the grid node and they are assumed constant over control volumes. This linearization yields:  $S_\phi = S_C + S_P\phi$ , where  $S_C = (1 - \gamma)(G + 3\phi^{*4})V_e + Q'''V_e$  and  $S_P = -4(1 - \gamma)\phi^{*3}V_e$ . Here,  $\phi^*$  is the value of the dependent variable,  $\phi$ , at the preceding step of the iterative solution procedure presented in Section 9 and  $V_e$  is the volume of the element.

In the source term integral of equation (8), the source term  $S_\phi = -I + S_I$  is linearized and assumed constant over control volumes and solid angles. Hence, for this dependent variable,  $S_C = \omega_m S_I^m V_e$  and  $S_P = -\omega_m V_e$ , where the subscript or superscript  $m$  indicates that the calculation is carried out for a particular direction  $\vec{\Omega}_m$ . A different representation of the distribution of  $S_\phi$  in the volumetric integral of equation (14) for radiation heat transfer, such as a linear variation over the elements, is possible but more complex to implement: it may also lead to coupling between directions that does not conform with the RTE [34]. To accelerate convergence, Chai et al. [38] proposed to extract from  $S_C$  the component of the in-scattering term that pertains to direction  $\vec{\Omega}_m$  and

to include it into  $S_P$ . This was indeed found to decrease the number of iterations required by the algorithm to converge.

### 6.3. Dependent variable $\phi$

Three interpolation schemes are required: one for diffusion, one for convection, and one for radiation heat transfer.

#### 6.3.1. Diffusion terms

The diffusive flux term, denoted  $\vec{J}_\phi^D$ , is discretized using a linear interpolation of  $\phi$  within each element [67]:

$$\phi^D = A_1^D x + A_2^D y + A_0^D \quad (17)$$

in which the superscript D refers to the interpolation function used in deriving an algebraic approximation for the transport of  $\phi$  by *diffusion*;  $x$ ,  $y$  are the spatial independent variables in a Cartesian coordinate system local to each element, with origin at the centroid; and  $A_n^D$  are the geometric constants.

Referring to the triangular element depicted in *figure 2*:  $A_0^D$  is the arithmetic mean of the nodal values of  $\phi$ ,  $A_1^D = \check{y}_j \phi_j / D$ , and  $A_2^D = \check{x}_j \phi_j / D$ , where  $\check{y}_n = (y_{\vartheta(n+1)} - y_{\vartheta(n+2)})$ ,  $\check{x}_n = (x_{\vartheta(n+1)} - x_{\vartheta(n+2)})$ , and  $D = (x_1 y_2 + x_2 y_3 + x_3 y_1 - x_2 y_1 - x_3 y_2 - x_1 y_3)$ .

Here and in the following paragraphs, the integer function  $\vartheta$  is defined such that:  $\vartheta(n) = n$ ,  $\forall n = 1, 2, 3$ , and  $\vartheta(n) = n - 3$ ,  $\forall n = 4, 5, 6$ .

An equivalent and perhaps more elegant development of this linear interpolation on triangular elements could be carried out using barycentric or area coordinates such as in FEMs. However, with such an approach, Delaunay triangulation is needed to ensure positive contributions to the algebraic discretization equations.

#### 6.3.2. Convection terms

The convective flux term, denoted by  $\vec{J}_\phi^C$ , can be discretized with a flow-oriented scheme such as that discussed by Baliga and Patankar [46], or using a skew mass-weighted scheme such as those introduced by Schneider and Raw [69] and then by Saabas [70] and Rouse [65].

The flow oriented (FLO) scheme is based on two main ideas: (1) it is defined with respect to a flow-oriented Cartesian coordinate system located at the centroid of the element; and (2) it takes into account the relative strengths of convection and diffusion via an element-based Peclet number,  $Pe_e$ .

In *figure 2*, a local flow-oriented Cartesian coordinate system  $(x, y)$  is located at the triangular-element centroid,  $O$ , so as to align the  $x$  axis with the element-average velocity vector,  $\vec{V}_{av}$ . The velocity is assumed to vary linearly within the element. Hence, the components of  $\vec{V}_{av}$  and its magnitude within this element are given by  $u_{av} = [U_1 + U_2 + U_3]/3$ ,  $v_{av} = [V_1 + V_2 + V_3]/3$ , and  $V_{av} = [u_{av}^2 + v_{av}^2]^{1/2}$ .

Assuming a uniform mean flow,  $\vec{V}_{av}$ , and no source term within an element, *only* for the purpose of obtaining guidance for a suitable interpolation function, the multi-dimensional distribution of a transported scalar throughout an element is governed by

$$\vec{\nabla} \cdot \vec{J}_e = \rho_e V_{av} \frac{\partial \phi}{\partial x} - \Gamma_e \left( \frac{\partial^2 \phi}{\partial x^2} + \frac{\partial^2 \phi}{\partial y^2} \right) = 0 \quad (18)$$

Introducing  $x_{\max} = \text{MAX}[x_1, x_2, x_3]$  and  $x_{\min} = \text{MIN}[x_1, x_2, x_3]$ , where the subscripts 1, 2 and 3 identify the three nodes of the triangular element, and an elemental Peclet number defined as

$$Pe_e = \frac{\rho_e V_{av} (x_{\max} - x_{\min})}{\Gamma_e} \quad (19)$$

a new independent variable,  $\xi$ , can be defined

$$\xi = \frac{\Gamma_e}{\rho_e V_{av}} \left\{ \exp \left[ \frac{Pe_e (x - x_{\min})}{(x_{\max} - x_{\min})} \right] - 1 \right\} \quad (20)$$

The FLO interpolation scheme is obtained by using a particular solution for the distribution of a transported scalar that satisfies equation (18):

$$\phi^C = A_1^C \xi + A_2^C y + A_0^C \quad (21)$$

In equation (21), the superscript C refers to the interpolation function used in deriving an algebraic approximation to the transport of  $\phi$  by *convection*. Referring to a local coordinate system located at the centroid of the triangular element depicted in *figure 2*:  $A_0^C = \check{\xi} y_j \phi_j / D$ ,  $A_1^C = \check{y}_j \phi_j / D$ , and  $A_2^C = \check{\xi}_j \phi_j / D$ , where  $\check{\xi}_n = \xi_{\vartheta(n+2)} - \xi_{\vartheta(n+1)}$ ,  $\check{y}_n = y_{\vartheta(n+1)} - y_{\vartheta(n+2)}$ ,  $\check{\xi} y_n = \xi_{\vartheta(n+1)} y_{\vartheta(n+2)} - \xi_{\vartheta(n+2)} y_{\vartheta(n+1)}$ , and  $D = (\xi_1 y_2 + \xi_2 y_3 + \xi_3 y_1 - \xi_2 y_1 - \xi_3 y_2 - \xi_1 y_3)$ .

In planar two-dimensional problems that involve acute-angled triangular elements and relatively low element-based Peclet number,  $Pe_e$ , the FLO scheme has proved quite successful. If high values of  $Pe_e$  are encountered, this interpolation function may lead to negative coefficients in the discretization equations. This difficulty is compounded when obtuse angled triangular elements

are used. Such negative coefficients introduce physically unrealistic net outflow of the dependent variable  $\phi$  from control volumes.

The donor cell scheme of Prakash [71] is one way of ensuring positive coefficients. Here, the author proposes to use a Skew Positive Coefficient Upwind (SPCU) scheme [65]. This SPCU interpolation scheme involves two main ideas: (1) the integrated convective flux across a panel  $p_l$  is approximated by an appropriately calculated mass flow rate,  $\dot{m}_l$ , times a suitable mean value of  $\phi$ ,  $\bar{\phi}_l$ , which is assumed to prevail over  $p_l$ ; and (2) the mean value of the dependent variable  $\bar{\phi}_l$  at  $p_l$  is a weighted average of the value of  $\phi$  at an upstream grid point,  $N$ , and the values of  $\bar{\phi}$  prevailing over the other panel surfaces inside the element under consideration.

Assuming that  $\bar{\phi}_1$  prevails over panel  $p_1$ , in *figure 2*, the integrated convective flux  $\vec{J}^C$  across the surface of  $p_1$  is approximated by

$$\int_{p_1} \vec{J}^C \cdot \vec{n}_1 dA = \dot{m}_1 \bar{\phi}_1 \quad (22)$$

where

$$\dot{m}_1 = \int_{p_1} \rho (\vec{V} \cdot \vec{n}_1) dA \quad (23)$$

The mass flow rate,  $\dot{m}_1$ , can be integrated exactly when an analytical function for the velocity distribution is provided. If only nodal values of  $\vec{V}$  are available, the mass flow rate is approximated by the product of the density,  $\rho$ , the surface area of  $p_1$  ( $A_1$ ), and an appropriately interpolated velocity,  $\vec{V}_{av}$ , at the centroid of  $p_1$ . This yields

$$\dot{m}_1 = \rho \vec{V}_{av} \cdot \vec{n}_1 A_1 \quad (24)$$

The ideas involved in the mass-weighted average of  $\phi$  are first outlined for sub-control volume  $V_1$  depicted in *figure 2*. Let the mass flow rate at panel two,  $\dot{m}_2$ , be positive, that is, its direction is aligned with the unit vector  $\vec{n}_2$ . Then, according to the proposed scheme,  $\bar{\phi}_2$  is given by a linear function of  $\bar{\phi}_3$  and  $\phi_1$ :

$$\bar{\phi}_2 = f_2^+ \bar{\phi}_3 + (1 - f_2^+) \phi_1 \quad (25)$$

To ensure a positive contribution to the coefficients when  $\dot{m}_3$  is *negative*—coming out of sub-control volume  $V_1$ —we need that  $\bar{\phi}_2 = \phi_1$ : the values of  $\bar{\phi}_2$  and  $\bar{\phi}_3$  at the panels  $p_2$  and  $p_3$  for this situation should only depend on the value of  $\phi$  at node 1, which is located upstream of these two surfaces: this implies that  $f_2^+ = 0$ . On the other hand, if  $\dot{m}_3$  is *positive*—coming into sub-control volume 1—

and greater than  $\dot{m}_2$ , only  $\bar{\phi}_3$  should influence the value of  $\bar{\phi}_2$ , because the amount of scalar transported by convection out of control volume  $V_1$  across panel  $p_2$  has to be greater than or equal to what comes in by convection through panel  $p_3$ , in order to ensure the positiveness of coefficients [65]. For this case  $f_2^+ = 1$ . In other situations, the function  $f_2^+$  is just the ratio of the mass flow rate coming into sub-control volume 1 through  $p_3$  to that going out through  $p_2$ . Consequently, a general expression for  $f_2^+$ , for a *positive*  $\dot{m}_2$  can be defined as

$$f_2^+ \equiv \text{MIN} \left[ \text{MAX} \left( \frac{\dot{m}_3}{\dot{m}_2}, 0 \right), 1 \right] \quad (26)$$

The subscript 2 stipulates the association with panel 2 and the superscript + indicates that  $\dot{m}_2$  is positive.

If these same guide lines are followed when the mass flow rate  $\dot{m}_2$  is flowing into sub-control volume  $V_1$ — $\dot{m}_2$  is *negative*—then an equation, involving node 3 and panel  $p_1$ , can readily be obtained such that

$$\bar{\phi}_2 = f_2^- \bar{\phi}_1 + (1 - f_2^-) \phi_3 \quad (27)$$

where  $f_2^-$  is defined as

$$f_2^- \equiv \text{MIN} \left[ \text{MAX} \left( \frac{\dot{m}_1}{\dot{m}_2}, 0 \right), 1 \right] \quad (28)$$

Introducing a second weighting function  $w_2$  defined as

$$w_2 \equiv \text{MAX} \left( \frac{\dot{m}_2}{|\dot{m}_2|}, 0 \right) \quad (29)$$

it is possible to account for the negative or positive value of  $\dot{m}_2$  by expressing  $\bar{\phi}_2$  as

$$\begin{aligned} \bar{\phi}_2 = & w_2 [f_2^+ \bar{\phi}_3 + (1 - f_2^+) \phi_1] \\ & + (1 - w_2) [f_2^- \bar{\phi}_1 + (1 - f_2^-) \phi_3] \end{aligned} \quad (30)$$

A general mathematical expression of  $\bar{\phi}$  at any of the three panels,  $p_1, p_2, p_3$ , can be arrived at, using the integer function  $\vartheta(n)$ , when the following general weighting functions are defined:

$$\begin{aligned} w_l & \equiv \text{MAX} \left( \frac{\dot{m}_l}{|\dot{m}_l|}, 0 \right) \\ f_l^+ & \equiv \text{MIN} \left[ \text{MAX} \left( \frac{\dot{m}_{\vartheta(l+1)}}{\dot{m}_l}, 0 \right), 1 \right] \\ f_l^- & \equiv \text{MIN} \left[ \text{MAX} \left( \frac{\dot{m}_{\vartheta(l+2)}}{\dot{m}_l}, 0 \right), 1 \right] \end{aligned} \quad (31)$$

with  $l = 1, 2, 3$  for panels  $p_1, p_2, p_3$ , respectively.

The general expression for  $\bar{\phi}_l$  is then

$$\begin{aligned} \bar{\phi}_l = & w_l [f_l^+ \bar{\phi}_{\vartheta(l+1)} + (1 - f_l^+) \phi_{\vartheta(l+2)}] \\ & + (1 - w_l) [f_l^- \bar{\phi}_{\vartheta(l+2)} + (1 - f_l^-) \phi_{\vartheta(l+1)}] \end{aligned} \quad (32)$$

Equation (32) is a system of three equations for the three unknowns,  $\bar{\phi}_l$ . The SPCU scheme ensures, at an elemental level, that algebraic approximations to the convective transport terms contribute positively to the coefficients of the discretization equations. The SPCU scheme is, however, highly implicit, which makes it not very amenable to use in conjunction with Newton-type linearizations. Here, this does not pose any difficulty as a successive-substitution solution method is used. It should also be noted that a  $3 \times 3$  matrix of the element-interpolation coefficients must be inverted to obtain the expressions of the dependent variables at the control-volume faces. In the implementation of the SPCU scheme, when the analytical velocity distribution is available, the mass flow rate across the control-volume surfaces (panels) can be calculated using: (1) linear interpolation of velocity; (2) Simpson's rule or Gaussian quadrature integration of velocity on a panel, with integration point values specified via the analytical profile; and (3) exact integration of the velocity profile. The exact integration respects mass conservation precisely—but this condition is not guaranteed by the other types of integration. However, in the test cases considered in [64], no significant gains in accuracy were observed using exact integration, not available in general, and because Euler integration of  $\phi$  also proved economical. The linear interpolation of velocity within each element is thus recommended. The appropriate formulation and validation of the SPCU scheme was carried out by comparing its performance with respect to the FLO scheme [64].

### 6.3.3. Radiation terms

The flux vector,  $\vec{J}_\phi$ , in the context of equation (8), can be assumed to point in the same direction over an entire solid angle, and its value assumed to prevail over it. This is analogous to an upwind-type of interpolation function used in approximation of integrals of convective flux over a surface in FVMs [67]. Thus, the left-hand side of equation (14) is approximated by

$$\int_{\omega_m} \int_A \vec{J} \cdot \vec{n} \, dA \, d\omega \approx \omega_m \int_A \vec{J}^m \cdot \vec{n} \, dA \quad (33)$$

The intensity of radiation is evaluated at the centroid of the panels of an element, and it is assumed to prevail over it. Then, equation (33) becomes

$$\begin{aligned} \omega_m \int_A \vec{J}^m \cdot \vec{n} \, dA &\approx \omega_m \sum_{l=1}^N (\vec{J}_{p_l}^m \cdot \vec{n}_l) A_l \\ &= \omega_m \sum_{l=1}^N I_l^m (\vec{\Omega}_m \cdot \vec{n}_l) A_l \end{aligned} \quad (34)$$

where  $N$  is the total number of panels defining a control volume,  $\vec{\Omega}_m$  is the discrete direction,  $n_l$  is the unit outward-pointing normal to a panel  $p_l$ ,  $A_l$  is the surface area of  $p_l$ , and  $I_l^m$  is the average intensity on  $p_l$  along  $\vec{\Omega}_m$ . One of the assumptions involved in equation (34) is that the dot product  $(\vec{\Omega}_m \cdot \vec{n}_l)$  is constant over  $\omega_m$ . In the CVFEM formulation, the integral of this quantity over all solid angles, for each panel  $p$  in the domain, can also be evaluated analytically when both the spatial and angular grids are specified. An azimuthal angular discretization is recommended with this approach. This more accurate treatment of that integral over solid angles, originally proposed by Chui [33], yields the following approximation:

$$\int_{\omega_m} \int_A \vec{J} \cdot \vec{n} \, dA \, d\omega \approx \sum_{l=1}^N I_l^m G_l^m A_l \quad (35)$$

where the geometric quantity  $G_l^m$  is

$$G_l^m = \int_{\omega_m} (\vec{\Omega} \cdot \vec{n}_l) \, d\omega \quad (36)$$

Theoretically, this should increase the accuracy of the approximation involved with equation (33). However, it was found that for the isotropic scattering problems investigated in the companion paper [64] (and for several others), with either formulations, no significant difference was detected in terms of accuracy.

In the context of a prevailing assumption:

$$G_l^m = \int_{\omega_m} (\vec{\Omega} \cdot \vec{n}_l) \, d\omega = \omega_m (\vec{\Omega}_m \cdot \vec{n}_l) \quad (37)$$

a closure relation is required to relate values of the intensity at integration points to the nodal values.

Three different closure relations were implemented. All of them relate integration points to a *single* nodal value. The involvement of a single nodal value of intensity to specify the value at the integration point could be challenged. However, the intensity  $I_r^m$  at a reference location  $r$  in figure 4 can hardly be evaluated from neighboring nodes A and B either, although this is common practice in the literature. Chui et al. [36] approximate  $I_r^m$  from surrounding nodal values—four neighboring

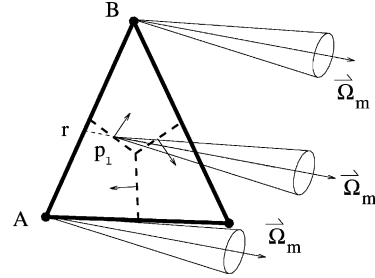


Figure 4. Influence of nodal values of intensity on control volume faces intensities.

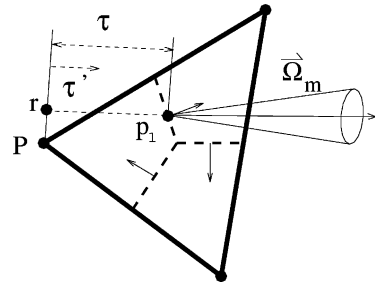


Figure 5. Attenuation scheme according to Bouguer's law: propagation from reference point  $r$  to integration point  $p_1$ .

nodes are involved—using bilinear interpolation, which is strictly no more physically sound than what is proposed here and yet more cumbersome. First, for specific directions, a node located *downstream* with respect to the integration point, may have an influence on the value of the intensity at this point. Second, in the context of two nodes of influence and when both nodes are located *upstream* with respect to the integration point, such as in figure 4, there is no guarantee that  $I_r^m$  will *physically* be a combination of the nodal values of intensity at A and B.

The three spatial interpolation schemes that were implemented are: the exponential scheme, the diffusion scheme, and the upwind scheme.

(1) The essence of the *exponential scheme* is that the values of  $I_{p_l}^m$  at the integration point on the panels are obtained by a one-dimensional integration of the RTE along the path  $\tau'$ , aligned with  $\vec{\Omega}_m$ , between a reference point  $r$  and the integration point  $p_l$  [65] (figure 5). With constant properties along the integration path  $\tau$  and constant source of radiant intensity  $S_I^m$ , this yields:  $I_{p_l}^m = I_r^m e^{-\tau} + S_I^m (1 - e^{-\tau})$ . This is equivalent to expressing  $S_I^m$  as the first term of a Taylor series expansion about the integration point  $p_l$ , along with the assumption that  $S_I^m$  equals  $S_{I_p}^m$ . The exponential scheme can be enhanced—leading to the *modified exponential scheme*—

by linearizing the equation of transfer, thus modifying the cell optical thickness  $\tau$ . This idea, proposed by Chai in the context of the DOM [38], was found to reduce the CPU time needed to achieve convergence of the CVFEM for scattering media, without compromising accuracy, especially when high optical thicknesses were involved. In this CVFEM, the reference point  $r$  is chosen to lie in a plane that involves only one grid point,  $P$ . This plane is referred to as the *isointensity* plane. The attenuation path and relations between node  $P$ , reference point  $r$ , and integration point  $p_l$  in a typical element are depicted in *figure 5*. Assuming, for the purpose of the interpolation function only, that the intensity along  $\Omega_m$  is constant in this plane yields:  $I_r^m = I_p^m$ .

(2) In the FVM formulation of Raithby and Chui [34], the authors suggested to keep an additional term of the above-mentioned Taylor series expansion, in order to capture the optically thick limit (diffusion approximation). For the problems investigated in the original work of Rousse [65] involving one-, two- and three-dimensional problems, no significant gain in accuracy was obtained except for optically thick media ( $\tau_0 \geq 10$ ). The proposed enhancement, although based on physical arguments, was found to moderately increase the CPU time required per iteration and dramatically augment the total number of iterations to obtain convergence. It was found computationally less expensive to use a simpler scheme with a finer grid than this *diffusion scheme*.

(3) The simplest scheme is the first-order accurate step or *upwind* scheme. Since no attenuation is experienced between the reference point and the integration point, this scheme produces physically realistic solutions on fine spatial grids only or when no attenuation occurs. In a one-dimensional context, there is an advantage to use a scheme that models the one-dimensional physics of radiative transfer more accurately. However, Chai et al. [39] recommended using the *upwind scheme* in Cartesian coordinates computations. With the *upwind scheme* the closure relation is simply,  $I_{p_l}^m = I_r^m = I_p^m$ , and the exact location of the point  $r$  is not critical as long as no attenuation is involved in the interpolation function.

Other popular schemes are the diamond scheme and its variations involving fix-up procedures for negative coefficients and others. These are not discussed here.

The so-called exponential scheme [13, 72, 73] is indeed a particular solution of the RTE in 1D. Hence, a parallel argument can be made with convection–diffusion numerical analyses in which one-dimensional solutions are used as interpolation functions in multi-dimensional contexts [67].

## 7. DISCRETIZATION EQUATIONS

The general discretization equation for  $\phi$  at a typical point  $P$  takes the form:

$$A_P \phi_P = \sum_{nb=1}^N A_{nb} \phi_{nb} + A_P^* \quad (38)$$

where  $N$  is the number of nodes surrounding  $P$ ,  $\phi_{nb}$  are the discrete values of the dependent variable evaluated at the grid points surrounding node  $P$ ,  $A$  are the coefficients of the algebraic discretization equations, and  $A^*$  accounts for the terms that do not explicitly involve  $\phi$ . One such equation is obtained when  $\phi$  stands for temperature and  $N$  equations must be solved for the intensity of radiation.

The discretization-equation coefficients for any CVFEM are obtained in two steps: (1) determination of element contributions to the coefficients of equation (38); and (2) assembly of these contributions for all sub-control volumes associated with a given node  $P$ . Implementation details are provided in [65] and are available upon request.

## 8. BOUNDARY CONDITIONS

For grid points that lie on the boundaries of the calculation domain, the assembly of internal element contributions is insufficient to establish conservation over the associated control volumes and solid angles: the transport of the dependent variable  $\phi$  across surfaces of the control volumes that coincide with domain boundaries has to be included. Algebraic approximations of the flux integrals on the boundaries are consequently required.

### 8.1. Energy equation

For the solution of equation (7), four types of boundary conditions can be considered in the proposed formulation [65]: (1) specified value; (2) specified gradient; (3) specified heat transfer coefficient and ambient temperature; and (4) specified nonlinear function of temperature. For grid points that lie on specified-value boundaries, the implementation of the boundary condition is simply done by overwriting the coefficients and setting  $A_P = 1$ ,  $A_{nb} = 0$ , and  $A_P^* = \phi_{\text{spec}}$ , after the assembly of internal element contributions. When the gradient of the dependent variable *normal* to the boundary is given, a suitable (Euler, Simpson, analytical) integration of this gradient and of the velocity normal to the boundary is

used in the evaluation of the convection–diffusion flux over the two sub-control volume surfaces that determine the boundaries. When the heat transfer coefficient  $h$  and the ambient temperature  $\phi_\infty$  are given for impermeable boundaries, nodal values of  $h$  and  $\phi_\infty$  are specified and assumed to prevail over the surface of a boundary control volume. When the flux at the boundary is given by a non-linear function of the dependent variable, this function is linearized as prescribed by Patankar [67], and the resulting expressions are assumed to prevail over the surface of the boundary control volume.

## 8.2. Radiative transfer equation

In this work, the radiative boundary conditions for gray-diffuse surfaces are specified in terms of a surface emissivity,  $\epsilon$ , in equation (11). Hence, two types of situations are considered to account for boundary conditions: (1) *impinging* radiation on a portion of the surface of a control volume that coincides with a boundary; and (2) *outgoing* radiation that accounts for emission and reflection of impinging radiation. An impinging directional heat rate,  $q_l^m$ , is calculated for each direction  $\vec{\Omega}_m$ , associated with a path that ends at a panel (control volume surface)  $p_l$ . In two-dimensional problems,  $l = 1, 2$  as shown in figure 6. The impinging directional heat rate at  $p_l$  over solid angle  $\omega_m$  is approximated by

$$q_l^m = I_{p_l}^m \tilde{G}_l^m A_l \quad (39)$$

where  $\tilde{G}_l^m$  represents the angular integral of  $(\vec{\Omega}_m \cdot \vec{n}_l)$  over the portion  $\tilde{\omega}_l^m$  of solid angle  $\omega_m$ : that is impinging and intercepted by the surface of  $p_l$ . Provision is then made to account for directions associated with solid angles that straddle over a boundary panel: such treatment is required when it is not possible to align the solid angle edges with the boundaries of the spatial calculation domain.

For a direction  $\vec{\Omega}_m$  that is pointing inside the calculation domain (outgoing with respect to the boundary surface), the discrete boundary condition at a boundary node B, along  $\vec{\Omega}_m$ , can be approximated by

$$I_B^m = \epsilon_B I_{bB} + 4(1 - \epsilon_B) \frac{q_B^{\text{in}}}{A_B} \quad (40)$$

where the black-body diffuse emission of energy,  $I_{bB}$ , is based on the fourth power of the absolute value of boundary temperature, and  $A_B$  corresponds to the surface area of the boundary of control volume  $V_B$  that receives radiation, and  $q_B^{\text{in}}$  is the total impinging heat

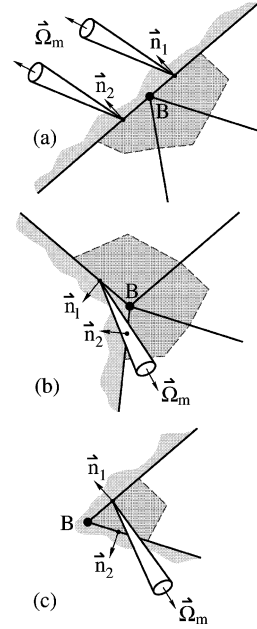


**Figure 6.** Boundary configurations in two dimensions: (a) aligned,  $\theta = 180^\circ$ ; (b) obtuse,  $\theta > 180^\circ$ ; (c) acute,  $\theta < 180^\circ$ .

rate on the surface of the boundary control volume associated with node B.  $q_B^{\text{in}}$  accounts for the above-mentioned impinging radiative heat rates,  $q_l^m$ , in all directions  $\vec{\Omega}_m$ , that impinge on the boundary and all control volume surfaces (panels),  $p_l$ , associated with node B. At the implementation level,  $q_B^{\text{in}}$  is based on the latest available information for all directions [65]. For reflective boundaries, the convergence is then slower than for black surfaces.

For a regular boundary surface such as that depicted in figure 6(a), both  $p_1$  and  $p_2$  have normals pointing in the same direction, and  $\tilde{A}_B$  is the sum of both surface areas,  $A_1$  and  $A_2$ , when radiation is impinging on B. For cases (b) and (c), for some directions, the vector  $\vec{\Omega}_m$  may either hit  $p_1$  and leave  $p_2$ , or vice versa. For example, in figure 6(b), only the fraction of the total incoming flux that is impinging on panel  $p_1$  is used as the total flux on the boundary to compute the intensity along  $\vec{\Omega}_m$ , and the surface area  $\tilde{A}_B$  is  $A_1$  only.

## 9. SOLUTION PROCEDURE

### 9.1. Nonlinearity

The combined-mode heat transfer equations are highly nonlinear. More nonlinearities could also be present

due to temperature dependent thermophysical and/or radiative properties. Hence, a successive-substitution linearization scheme (Picard iteration), in which coefficients are computed using the latest available values of the dependent variables, is employed.

## 9.2. Storage and convergence rates

With an iterative method, relatively small storage is required as algebraic coefficients for the different variables involved do not have to be stored in memory at the same time. This feature is especially important in three-dimensional combined-modes problems. A successive-substitution linearization scheme is also appropriate as the convergence rate and convergence criteria for each variable may differ. Indeed, the required level of convergence *in each iteration* for the intensity of radiation and the temperature are often different.

## 9.3. Relaxation

The nonlinearities in the discretization equations may lead to large changes in the predicted solutions between successive iterations. These changes may cause oscillations and/or divergence in the iterative process. This problem can be overcome by the use of relaxation techniques [65]. When solving for intensity, it was found that over-relaxation accelerates convergence of the algorithm especially for high optical thickness.

## 9.4. Marching techniques

When there is no scattering, the source function  $S_I$  in equation (8) is temperature dependent only, and the intensity along a given direction becomes independent of intensities in other directions. For these cases,  $S_I$  could be calculated prior to the iterative process. Furthermore, when all boundary surfaces are black, the discretization equations could be solved by marching techniques (the emitted flux at the boundaries is independent of the incoming radiation). This was not implemented here, as an iterative solution can strategically be used whether or not either one or both of these two conditions is respected. The choice of an iterative technique is also justified for irregular domains where mapping is required in marching techniques to visit each element in an appropriate sequence.

## 10. CONCLUSION

A CVFEM for combined conduction–convection–radiation heat transfer in two-dimensional planar regularly- or irregularly-shaped geometries, filled with emitting, absorbing, and scattering media, has been presented in detail in this paper.

### 10.1. Contributions

Contributions of this work include the following: (1) a CVFEM for two-dimensional combined modes of heat transfer; (2) a CVFEM that uses the same coefficient assembly and solution procedure for convective and radiative transport; (3) a CVFEM for the solution of the RTE on equally divided triangular finite elements; and (4) a first order skew positive coefficient upwind (SPCU) scheme of interpolation for the calculation of convective transport and its implementation on equally divided triangular finite elements.

### 10.2. Key features

Globally: (1) the formulations proposed here can be extended and combined to CVFEMs for problems involving fluid flow calculations that use the same non-orthogonal computational grids; (2) the formulations were designed to allow for the maximum flexibility; and (3) irregular domains can be considered.

In the context of convection–diffusion: (1) the formulation of the SPCU scheme for equally subdivided triangular elements was implemented to guarantee positive coefficients in the discretized algebraic equations; (2) the FLOW Oriented (FLO) scheme was also implemented and can be used when nondistorted grids are employed as long as no negative coefficients are encountered; and (3) other interpolation functions can be implemented (for example, a combination of the FLO and SPCU scheme can be used to avoid negative coefficients and still ensure high accuracy).

In view of radiative transfer calculations: (1) the angular integral of  $(\vec{\Omega} \cdot \vec{n})$  over  $\omega$  can be handled in two different manners; (2) the formulation can use different angular discretizations; (3) emission, absorption, and scattering can be considered; and (4) several interpolation functions can be incorporated into this formulation.

### 10.3. Recommendations

Here are some of the issues which deserve special attention: (1) modifications should be incorporated in the SPCU scheme to enhance its capabilities to approximate the influences of the direction and strength of the flow within an element; (2) the ideas involved with the SPCU scheme should be implemented and tested in the context of radiation heat transfer; (3) the CVFEM for radiation heat transfer should be extended to account for non-gray media and anisotropic scattering; and (4) the CVFEM for combined modes of heat transfer should be formulated for implementation on parallel algorithms.

During the testing of the proposed CVFEM, it was noted that several numerical improvements could also be incorporated to increase its efficiency. Some suggested improvements are presented in the concluding remarks of the companion paper [64].

#### Acknowledgement

The author gratefully acknowledges EDF for its support and the Natural Sciences and Engineering Research Council for an operating research grant.

### REFERENCES

- [1] Hottel H.C., Cohen E.S., Radiant heat exchanges in gas-filled enclosure: Allowance for nonuniformity of gas temperature, *AIChE J.* 4 (1958) 3–14.
- [2] Hottel H.C., Sarofim A.F., *Radiative Transfer*, McGraw-Hill, New York, 1967.
- [3] Howell J.R., Application of Monte Carlo method to heat transfer problems, *Adv. Heat Transfer* 5 (1969).
- [4] Haji-Sheikh A., Monte-Carlo methods, in: Minkowycz W.J., Sparrow E.M., Schneider G.E., Pletcher R.H. (Eds.), *Handbook of Numerical Heat Transfer*, Chapter 16, Wiley & Sons, New York, 1988, pp. 421–461.
- [5] Halton J.H., A retrospective and prospective review of the Monte-Carlo method, *SIAM Rev.* 12 (1) (1990) 1–63.
- [6] Sakami M., Charette A., Le Dez V., Application of the discrete ordinates method to combined conductive and radiative heat transfer in a two-dimensional complex geometry, *J. Quant. Spectrosc. Radiat. Transfer* 56 (1996) 517–533.
- [7] Mengüç M.P., Viskanta R., Radiative transfer in three-dimensional rectangular enclosures containing inhomogeneous, anisotropically scattering media, *J. Quant. Spectrosc. Radiat. Transfer* 33 (1985) 533–549.
- [8] Shah N., The computation of radiation heat transfer, PhD Thesis, Imperial College, London, 1979.
- [9] Meng F.L., McKenty F., Camarero R., Radiative heat transfer by the discrete transfer method using an unstructured mesh, in: *HTD-Vol. 244, Radiative Heat Transfer: Theory and Applications*, ASME, 1993, pp. 55–66.
- [10] Carvalho M.G., Farias T., Fontes P., Predicting radiative heat transfer in absorbing, emitting, and scattering media using the discrete transfer method, in: *HTD-Vol. 160, Fundamentals of Radiation Heat Transfer*, ASME, 1991, pp. 17–26.
- [11] Selçuk N., Kayakol N., Evaluation of discrete transfer for radiative transfer in combustors, in: *Proc. Int. Symp. Radiative Transfer*, Kuşadaşı, Turkey, 1995.
- [12] Chandrasekhar S., *Radiative Transfer*, Clarendon Press, Oxford, 1950.
- [13] Carlson B.G., Lathrop, K.D., Transport theory—the method of discrete-ordinates, in: *Computing Methods in Reactor Physics*, Gordon and Breach, New York, 1968.
- [14] Hyde D.J., Truelove J.S., The discrete ordinates approximation for multidimensional radiant heat transfer in furnaces, Technical Report, UKAEA Report No. AERE-R8502, 1976.
- [15] Fiveland W.A., Discrete-ordinates solutions of the radiative transport equation for rectangular enclosures, *ASME J. Heat Tran.* 106 (2) (1984) 699–706.
- [16] Ramankutty M.A., Crosbie A.L., Modified discrete ordinates solution of radiative transfer in two-dimensional rectangular enclosures, *J. Quant. Spectrosc. Radiat. Transfer* 57 (1997) 107–140.
- [17] Selçuk N., Kayakol N., Evaluation of discrete ordinates method for radiative transfer in rectangular furnaces, *Int. J. Heat Mass Tran.* 40 (2) (1997) 213–222.
- [18] Fiveland W.A., Discrete-ordinate methods for radiative heat transfer in isotropically and anisotropically scattering media, *ASME J. Heat Tran.* 109 (3) (1987) 809–812.
- [19] Fiveland W.A., Three-dimensional radiation heat transfer solutions by discrete ordinates methods, *J. Thermophys. Heat Tran.* 2 (1988) 309–314.
- [20] Jamaluddin A.S., Smith P.J., Predicting radiative transfer in rectangular enclosures using the discrete ordinates method, *Combust. Sci. Tech.* 59 (1988) 321–340.
- [21] Kim T.K., Menart J.A., Lee H.S., Nongray radiative gas analysis using the  $S_n$  discrete ordinates method, *ASME J. Heat Tran.* 113 (1991) 946–952.
- [22] El Wakil N., Sacadura J.F., Some improvements of the discrete ordinates method for the solution of the radiative transport equation in multidimensional anisotropically scattering media, in: *HTD-Vol. 203, Developments in Radiative Heat Transfer*, ASME, 1992, pp. 119–127.
- [23] Fiveland W.A., Jessee J.P., Finite element formulation of the discrete ordinates method for multidimensional geometries, *J. Thermophys. Heat Transfer* 8 (1994) 427–433.
- [24] Jamaluddin A.S., Smith P.J., Predicting radiative transfer in axisymmetric cylindrical enclosures using the discrete ordinates method, *Combust. Sci. Tech.* 62 (1988) 173–186.
- [25] Jamaluddin A.S., Smith P.J., Discrete ordinates solution of the radiative transfer equation in non-axisymmetric cylindrical enclosures, *J. Thermophys. Heat Transfer* 6 (1992) 242–245.
- [26] Abraham J., Magi V., Application of the discrete ordinates method to compute radiant heat loss in a diesel engine, *Numer. Heat Transfer A* 31 (1997) 597–610.
- [27] Liou B., Wu C., Composite discrete ordinates solutions for radiative transfer in a two layer medium with Fresnel interfaces, *Numer. Heat Transfer A* 30 (1996) 739–751.

- [28] Liu J., Shang M., Chen Y.S., Prediction of radiative transfer in general body-fitted coordinates, *Numer. Heat Transfer B* 31 (1997) 423–439.
- [29] Liu J., Shang M., Chen Y.S., Wang T.S., Analysis of discrete ordinates method with even parity formulation, *J. Thermophys. Heat Transfer* 11 (1997) 253–261.
- [30] Liu J., Chen Y.S., Examination of conventional and even parity radiative transfer equations in irregular geometries, in: *Proc. Joint ASME/AIAA Thermophys. Heat Trans. Conf.*, Albuquerque, 1998, pp. 103–112.
- [31] Vaillon R., Lallemand M., Lemonnier D., Radiative heat transfer in orthogonal curvilinear coordinates using the discrete ordinates method, *J. Quant. Spectrosc. Radiat. Transfer* 55 (1) (1996) 7–17.
- [32] Charette A., Sakami M., Le Dez V., Analysis of radiative heat transfer in enclosures of complex geometry using the discrete ordinates method, in: *International Symposium on Radiative Transfer*, Kuçadaşi, Turkey, 1997.
- [33] Chui E.H., Modelling of radiative heat transfer in participating media by the finite volume method, PhD Thesis, University of Waterloo, Canada, 1990.
- [34] Raithby G.D., Chui E.H., A finite-volume method for predicting radiant heat transfer in enclosures with participating media, *ASME J. Heat Tran.* 112 (2) (1990) 415–423.
- [35] Chui E.H., Raithby G.D., Improved convergence rate in radiative transfer, *Numer. Heat Transfer B* 22 (1992) 251–272.
- [36] Chui E.H., Raithby G.D., Hughes P.M.J., Prediction of radiative transfer in cylindrical enclosures with the finite volume method, *J. Thermophys. Heat Transfer* 6 (1992) 605–611.
- [37] Chui E.H., Raithby G.D., Computation of radiant heat transfer on a non-orthogonal mesh using the finite volume method, *Numer. Heat Transfer B* 23 (1993) 269–288.
- [38] Chai J.C., Lee H.S., Patankar S.V., Improved treatment of scattering using the discrete ordinates method, *ASME J. Heat Tran.* 116 (1994) 260–263.
- [39] Chai J.C., Patankar S.V., Lee H.S., Evaluation of spatial differencing practices for the discrete-ordinates method, *J. Thermophys. Heat Transfer* 8 (1) (1994) 140–144.
- [40] Chai J.C., Lee H.S., Patankar S.V., Finite-volume method for radiation heat transfer, *J. Thermophys. Heat Transfer* 8 (1994) 419–425.
- [41] Chai J.C., Lee H.S., Patankar S.V., Treatment of irregular geometries using a cartesian coordinates finite-volume radiation heat transfer procedure, *Numer. Heat Transfer B* 26 (1994) 225–235.
- [42] Chai J.C., Parthasarathy G., Lee H.S., Patankar S.V., Finite-volume radiative heat transfer procedure for irregular geometries, *J. Thermophys. Heat Transfer* 9 (1995) 410–415.
- [43] Chai J.C., Moder J.P., Spatial-multiblock procedure for radiation heat transfer, *Numer. Heat Transfer* 31 (1997) 277–294.
- [44] Sanchez A., Smith T.F., Surface radiation exchange for two-dimensional rectangular enclosures using the discrete ordinates method, *ASME J. Heat Tran.* 114 (1992) 465–472.
- [45] Adams B.R., Smith P.J., Three-dimensional discrete ordinates modeling of radiative transfer in industrial-scale furnaces, in: *HTD-Vol. 203*, ASME, 1992, pp. 137–144.
- [46] Baliga B.R., Patankar S.V., A new finite-element formulation for convection-diffusion problems, *Numer. Heat Transfer* 3 (1980) 393–409.
- [47] Ferguson W.J., Turner I.W., Control volume finite element model of mechano-sorptive creep in timber, *Numer. Heat Transfer A* 29 (1996) 147–164.
- [48] Larreteguy A.E., An equal-order control volume finite element method for fluid flow in arbitrary triangulation, *Numer. Heat Transfer B* 28 (1995) 401–413.
- [49] Padra C., Larreteguy A.E., A-posteriori error estimator for the control volume finite element method as applied to convection-diffusion problems, *Numer. Heat Transfer B* 27 (1995) 63–80.
- [50] Harms T.M., Backström T.W., Prieur du Plessis J., Simplified control-volume finite element method, *Numer. Heat Transfer B* 30 (1996) 179–196.
- [51] Comini G., Malisan M., Manzan M., Accuracy comparison of control volume and Bubnov-Galerkin finite element methods for heat conduction problems, *Numer. Heat Transfer B* 29 (1) (1996) 43–60.
- [52] Prakash C., Baliga B.R., Control-volume-based numerical methods for fluid flow: Similarities and differences, in: Chung T.J., Karr G.R. (Eds.), *Finite Element Analysis in Fluids*, UAH Press, Huntsville, 1989.
- [53] Rousse D.R., Baliga R.B., Formulation of a control-volume finite element method for radiative transfer in participating media, in: *Proc. 7th Int. Conf. Numer. Meth. Thermal Problems*, Stanford, 1991, pp. 786–795.
- [54] Rousse D.R., Baliga R.B., Radiation heat transfer in an absorbing, emitting and scattering medium, in: *Proc. 4th Int. Conf. Nonlinear Eng. Comp.*, Swansea, 1991, pp. 639–648.
- [55] Rousse D.R., Baliga R.B., A control-volume finite element method for combined conduction-convection-radiation heat transfer, in: *Proc. 9th Gamm Conf. Num. Meth. Fluid Mechanics*, Lausanne, 1991, pp. 338–346.
- [56] Rousse D.R., Numerical method for conduction-convection-radiation heat transfer in three-dimensional geometries, in: *Proc. 2nd European Thermal Sciences and 14th UIT Conference*, Vol. 3, Rome, 1996, pp. 1425–1432.
- [57] Rousse D.R., Le couplage d'une méthode pour prédire le rayonnement avec les codes de CFD: Capacités et limitations d'une CVFEM, in: *Compte-rendus du congrès de la Société Française des Thermiciens*, Toulouse, 1997, pp. 538–544.
- [58] Rousse D.R., Gautier G., Sacadura J.F., A control volume finite element method for radiative heat transfer in irregular geometries, in: *Proc. 1998 AIAA/ASEM Thermophysics and Heat Transfer Conference*, Albuquerque, 1998, pp. 93–102.
- [59] Rousse D.R., Gautier G., Sacadura J.F., An updated CVFEM for radiative heat transfer in irregular geometries, in: *Proc. 1998 CSME Forum—Thermal and Fluids Engineering*, Toronto, 1998, pp. 379–386.
- [60] Rousse D.R., Gautier G., A CVFEM for combined modes of heat transfer in two-dimensional geometries, in: *Proc. 6th Annual CFD Conference*, Quebec, 1998, pp. XV27–XV33.

[61] Truelove J.S., Discrete-ordinate solutions of the radiation transport equation, ASME J. Heat Tran. 109 (4) (1987) 1048-1052.

[62] Baliga B.R., A control volume based finite-element method for convective heat and mass transfer, PhD Thesis, University of Minnesota, Minneapolis, 1978.

[63] Baliga B.R., Patankar S.V., A control volume finite-element method for two-dimensional fluid-flow and heat transfer, Numer. Heat Transfer 6 (1983) 245-261.

[64] Rouse D.R., Gautier G., Sacadura J.F., Numerical predictions of two-dimensional conduction, convection, and radiation heat transfer II. Validation, Int. J. Therm. Sci. (2000) (to be published).

[65] Rouse D.R., Numerical predictions of multidimensional conduction, convection, and radiation heat transfer in participating media, PhD Thesis, McGill University, Montréal, 1994.

[66] Siegel R., Howell J.R., Thermal Radiation Heat Transfer, 3rd edition, Taylor & Francis Ltd., London, 1992.

[67] Patankar S.V., Numerical Heat Transfer and Fluid Flow, Hemisphere, Washington, 1980.

[68] Finlayson B.A., The Method of Weighted Residuals and Variational Principles, Academic Press, New York, 1972.

[69] Schneider G.E., Raw M.J., A skewed positive influence coefficient upwinding procedure for control volume based finite element convection diffusion computation, Numer. Heat Transfer 9 (1986) 1-26.

[70] Saabas H.J., A CVFEM for three-dimensional, incompressible, viscous fluid flow, PhD Thesis, McGill University, Montréal, 1991.

[71] Prakash C., Examination of the upwind (donor-cell) formulation in control volume finite-element methods for fluid flow and heat transfer, Numer. Heat Transfer 11 (1987) 401-416.

[72] El Wakil N., Étude du transferts de chaleur par conduction, convection et rayonnement couplés dans les milieux semi-transparents fluides ou poreux, PhD Thesis, Institut National des Sciences Appliquées, Lyon, France, 1991.

[73] Lathrop K.D., Spatial differencing of the transport equation: Positivity vs accuracy, J. Comput. Phys. 4 (1969) 475-498.